Metal-insulator transition in cluster dynamical mean field theory: Intersite correlation, cluster size, interaction strength, and the location of the transition line

Chungwei Lin[1] and Andrew J. Millis[2]
[1]*Department of Physics and Astronomy, University of Pittsburgh, 3941 O'Hara St, Pittsburgh, Pennsylvania, 15260, USA*
[2]*Department of Physics, Columbia University, 538 W 120th Street, New York, New York 10027, USA*
(Received 19 December 2008; revised manuscript received 7 March 2009; published 14 May 2009)

To gain insight into the physics of the metal-insulator transition and the effectiveness of cluster dynamical mean field theory (DMFT) we have used 1, 2-, and 4-site dynamical mean field theory to solve a polaron model of electrons coupled to a classical phonon field. The metal to polaronic insulator phase boundary is determined along with electron spectral functions and cluster correlation functions. Pronounced cluster size effects occur in the intermediate coupling region in which the cluster calculation leads to a gap and the single-site approximation does not. Differences in spectra (in particular a sharper band edge in the cluster calculation) persist in the strong-coupling regime. A partial density of states is defined encoding a generalized nesting property of the band structure; variations in this density of states account for differences between the dynamical cluster approximation and the cellular-DMFT implementations of cluster DMFT, as well as for differences in behavior between the single-band models appropriate for cuprates and the multiband models appropriate for manganites. A pole or strong resonance in the self-energy is associated with insulating states; the momentum dependence of the pole is found to distinguish between Slater-like and Mott-like mechanisms for metal-insulator transition. Implications for the theoretical treatment of doped manganites are discussed.

DOI: 10.1103/PhysRevB.79.205109 PACS number(s): 71.38.−k, 71.30.+h

I. INTRODUCTION

Correlation-driven metal-insulator transitions are one of the fundamental issues in electronic condensed-matter physics.[1] It has known for many years that in models of electrons moving on a periodic lattice and subject to short-ranged interactions, insulating phases may occur if the number of electrons per unit cell, N, is an integer or rational fraction. If N is an even integer, then the Pauli principle makes insulating behavior possible even in the absence of electron-electron interactions (this is the case of filled bands). If N is not an even integer, interactions are required to obtain an insulator. Interactions may lead to a spontaneous breaking of translational symmetry, implying a unit cell larger by a factor of λ than the crystallographic cell. If λ is such that λN is an even integer, insulating behavior is clearly possible; this is referred to as the "Slater mechanism."[2] On the other hand insulating behavior may occur for N not an even integer even in the absence of spontaneous translational symmetry breaking. This is often termed the "Mott mechanism."[3]

Important insights into metal-insulator transition physics have come with the development of dynamical mean field theory (DMFT).[4] Single-site dynamical mean field theory, which entirely neglects spatial correlations in the electron gas, is found to predict a zero-temperature metal-insulator transition as the local interaction U exceeds a critical strength $U_c^{\text{single-site}}$ at density $N=1$.[4] More recently, cluster dynamical mean field theories[5–7] which include some degree of intersite correlations have been shown to produce metal-insulator transitions at much smaller values of U ($\sim 0.4 U_c^{\text{single-site}}$ when density $N=1$). However, the physics of the metal-insulator transition observed in the cluster-DMFT methods remains imperfectly understood, in part, because of the substantial computational expense of studying fully quantum cluster models.

In this paper we present results of a systematic cluster-DMFT study of a computationally simple polaron model, involving electrons coupled by an on-site density coupling to a dispersionless classical oscillator. The model exhibits spectra and metal-insulator phase diagrams similar to those of the interacting electron models of primary physical interest, but allows an extensive analysis. In particular, because quantum Monte Carlo calculations are not required, extensive simulations can be performed. Further, the model can be solved directly on the real axis, allowing access to spectra without the uncertainties of analytical continuation. We are able to determine the relation between short-ranged correlations and the metal-insulator phase boundary, elucidate the role of poles in the self energy, determine the minimum cluster size needed to see the effects of short-ranged interaction, and clarify the origin of the differences between dynamical cluster approximation (DCA) and cellular-DMFT approaches. However, clusters of size $N>4$ are not computationally accessible to us so while a cluster size dependence is observed, the issue of convergence to the lattice is not addressed.

The rest of this paper is organized as follows. In Sec. II we present the formalism we will use. We introduce the quantity "partial density of states" (PDOS) which is very important in determining the importance of short-ranged effects. In Sec. III we review the polaron model, give some calculational details related to the impurity cluster problem, and discuss different theoretical ways to measure the strength of short-ranged correlation. In Sec. IV we compare the results of 1-, 2-, and 4-site cluster approaches applied to the half-filled model. In particular we show that the momentum dependent poles in self-energies is the key to reduce the critical gap opening U. Section V concerns how the poles in self-energies depend on the temperature and interaction strength. In Sec. VI we discuss doping dependence and give a criterion on the minimal cluster size required to capture

short-ranged charge ordering effects. In Sec. VII we compare the results from DCA and cellular-DMFT, and from manganite and cuprate bands to illustrate the role of the partial density of states in cluster-DMFT calculations. Finally in a conclusion we summarize our results and discuss their implications. Two appendices give details of partial density of states and strong-coupling calculations.

II. GENERAL FORMALISM OF CLUSTER DMFT

A. Overview

In this section we review the general formalism for cluster dynamical mean field theory and give the equations for two frequently used approaches—cellular DMFT (CDMFT) (Ref. 8) and DCA,[9] and define a PDOS used in subsequent analysis. Special attention is paid to the 2-site and 4-site DCA formalisms on the square and cubic lattice. The main focus of this section is on the self-consistency condition.

B. Cluster dynamical mean field formalism

In an N_s-site cluster-DMFT calculation, one solves a quantum impurity model which may be described as an N_s-site cluster coupled to a noninteracting electron bath. The solution is expressed in terms of the impurity Green's function and self-energy—$\hat{G}^{\rm imp}$ and $\hat{\Sigma}^{\rm imp}$, which are $N_s \times N_s$ matrices in the space of cluster labels. The dynamical mean field step requires relating components of $\hat{G}^{\rm imp}$ and $\hat{\Sigma}^{\rm imp}$ to some combinations of lattice Green's functions and self-energies. There are two frequently used algorithms: the cellular-DMFT approach which is defined in real space and the DCA approach defined in momentum space.

In the cellular DMFT to a given lattice, one chooses an N_s-site supercell which periodically tiles the lattice and writes the Green's function as a matrix in this supercell, with entries depending on momentum $\vec{k}$ in the reduced Brillouin zone (RBZ) of the supercell lattice. One identifies sites of the quantum impurity model with sites of the supercell and takes interactions of the quantum impurity model to be those of the original model, but confined to a supercell. The self-consistency equation is

$$\hat{G}^{\rm imp} = \int_{\vec{k}\in {\rm RBZ}} (dk)[\omega + \mu - \hat{t}_{\vec{k}} - \hat{\Sigma}^{\rm imp}]^{-1} \tag{1}$$

with $(dk)=(d^dk)/(2\pi)^d$, RBZ stands for the reduced Brillouin zone, and $\hat{t}_{\vec{k}}$ is the $N_s \times N_s$ hopping matrix expressed in the basis of enlarged cell. In this approach the self-consistency equation is $\hat{G}^{\rm imp}_{ij} = G^{\rm lat}(\vec{R}_i - \vec{R}_j)$ with $\{\vec{R}\}$ basis vectors of the enlarged cell. The cellular-DMFT method breaks the lattice translational symmetry because the intersite correlations (expressed in $\hat{\Sigma}^{\rm imp}_{ij}$) within a supercell are *different* from those between supercells. After the cellular-DMFT equations are solved one may restore the translation invariance by periodizing the self-energy. Different methods have been proposed;[10] the issue is however not relevant to the considerations of this paper.

The DCA approximation is constructed in momentum space. One tiles the Brillouin zone into N_s equal area nonoverlapping tiles which we label by the average momentum $\vec{K}_i$. One approximates the self-energy $\Sigma(\vec{k},\omega)$ by $\Sigma_{\vec{K}_i}(\omega)$ if $\vec{k}$ is in the tile corresponding to $\vec{K}_i$. The *impurity* cluster model is defined by states labeled by the discrete set of labels $\vec{K}_i$; the impurity model interaction is taken to be the momentum-space lattice interaction $U_{\vec{k}_1\vec{k}_2\vec{k}_3\vec{k}_4}$ but with wave vectors restricted to the set $\vec{K}_i$. In the K_i basis the impurity model is diagonal and the self-consistency equation is

$$G^{\rm imp}_{\vec{K}_i}(\omega) = N_s \int_{\vec{p}\in i} (dp) \frac{1}{\omega + \mu - \epsilon_{\vec{p}} - \Sigma_{\vec{K}_i}(\omega)}. \tag{2}$$

Similar to single-site DMFT, it is useful to define the PDOS for each $\vec{K}_i$ sector as

$$D_i(\epsilon) = N_s \int_{\vec{p}\in \vec{K}_i} (dp)\, \delta(\epsilon - \epsilon_{\vec{p}}) \tag{3}$$

[note that the prefactor N_s leads to $\int d\epsilon D_i(\epsilon)=1$]. Once the PDOS is given, the self-consistency equation is

$$G^{\rm imp}_{\vec{K}_i}(\omega) = \int d\epsilon \frac{D_i(\epsilon)}{\omega + \mu - \epsilon - \Sigma^{\rm imp}_{\vec{K}_i}(\omega)}. \tag{4}$$

In all cases we have studied, the $\vec{K}_i$ basis diagonalizes the cellular-DMFT impurity model (G and Σ) also. Therefore the cellular-DMFT self-consistency condition can be expressed in the form of Eq. (2) with a different PDOS $D_i(\epsilon)$. An example is given in Appendix A (see also Refs. 11 and 12). We stress that the partial density of states is the only lattice information required in the cluster-DMFT equations. Different cluster schemes lead to different PDOS which is the mathematical origin of the different results.

One notices that if all partial density of states are identical to the total density of states $D(\epsilon)=D_i(\epsilon)$, the single-site DMFT solution also solves the DCA equations because the self-consistent equation for single-site DMFT $G^{\rm imp}(\omega) = \int d\epsilon \frac{D(\epsilon)}{\omega+\mu-\epsilon-\Sigma^{\rm imp}(\omega)}$ is identical to Eq. (4) for all $\vec{K}_i$ sectors. In this situation, $\Sigma^{\rm imp}_{\vec{K}_i}$ is identical for all $\vec{K}_i$ (Σ is purely local). A natural expectation is therefore that the separation between different sectors of PDOS indicates the degree of the short-ranged correlation. In the subsequent sections we show that this is indeed the case.

While the DCA is naturally formulated in the cluster momentum basis $\vec{K}_i$, it is often convenient to define a real-space basis by introducing a set of vectors $\{\vec{R}\}_{i=1\sim N_s}$ satisfying

$$\delta_{i,j} = \frac{1}{N_s} \sum_{l=1}^{N_s} e^{i(\vec{K}_i - \vec{K}_j)\cdot \vec{R}_l} \tag{5}$$

(in this basis the on-site interaction term in the impurity model is identical to that in the original lattice problem). Note that the $\{\vec{R}_i\}$ are only determined up to a uniform translation $\{\vec{R}_i\} \to \{\vec{R}_i + \vec{A}\}$ with $\vec{A}$ a lattice vector. Equation (5)

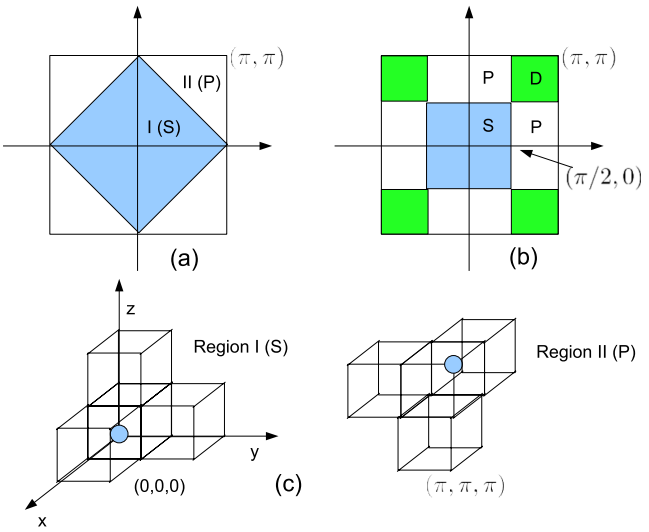

FIG. 1. (Color online) Partition of the Brillouin zone. (a) 2-site DCA on square lattice. (b) 4-site DCA on square lattice. (c) 2-site DCA on cubic lattice.

enables one to get real-space components from the impurity problem by the discrete Fourier transform

$$\Sigma^{\rm imp}_{\vec{R}_m}(\omega) = \frac{1}{N_s}\sum_{i=1}^{N_s} e^{-i\vec{K}_i\cdot\vec{R}_m}\Sigma^{\rm imp}_{\vec{K}_i}(\omega),$$

$$G^{\rm imp}_{\vec{R}_m}(\omega) = \frac{1}{N_s}\sum_{i=1}^{N_s} e^{-i\vec{K}_i\cdot\vec{R}_m}G^{\rm imp}(\vec{K}_i,\omega), \tag{6}$$

where $\Sigma^{\rm imp}(\vec{R}_m)=\Sigma^{\rm imp}_{i,i+m}$ and $G^{\rm imp}(\vec{R}_m)=G^{\rm imp}_{i,i+m}$. For each quantity, like the Green's function G, self-energy Σ, and Weiss function a, there are momentum and real-space components labeled by some subscript. In this paper, the real-space component is labeled by a number (0:on-site, 1:nearest neighbor) while the momentum-space sectors labeled by capital letters (S, P, D).

In cellular DMFT, different choices of N_s-site supercell are possible. In DCA different tilings of the Brillouin zone are possible. A comparative survey of the different choices has not been undertaken and would be worthwhile. It is natural to expect that tilings should respect the point symmetry of the lattice as much as possible, i.e., if the lattice remains invariant under the transform $\vec{r}\to\vec{r}'=U\vec{r}$, the ideal tiling of the Brillouin zone obeys $\Sigma(\vec{k})=\Sigma(U^{-1}\vec{k})$. In this paper we consider the particular 2-site and 4-site tilings on square and cubic lattices plotted in Fig. 1.

C. Formalism for 2-site DCA in square lattice

After solving the 2-site impurity problem, one gets (in the real-space basis)

$$\hat{G}^{\rm imp} = \begin{pmatrix} G_0 & G_1 \\ G_1 & G_0 \end{pmatrix} \hat{\Sigma}^{\rm imp} = \begin{pmatrix} \Sigma_0 & \Sigma_1 \\ \Sigma_1 & \Sigma_0 \end{pmatrix}. \tag{7}$$

The partitioning of Brillouin zone in this case is given in Fig. 1(a) so the two $\vec{K}$ points according to this division is $\vec{K}_{\rm I}=0$ and $\vec{K}_{\rm II}=(\pi,\pi)$. We label region I and II or S and P sectors. Corresponding to $\vec{K}_{\rm I}$ and $\vec{K}_{\rm II}$, one gets $\vec{R}_0=0$ and $\vec{R}_1=(\pm1,0)$ or $(0,\pm1)$ from the requirement Eq. (5). The lattice self-energy is related to $\hat{\Sigma}^{\rm imp}$ by

$$\Sigma_{\rm DCA}(\vec{k},\omega) = \begin{cases} \Sigma^{\rm imp}_S = \Sigma_0 + \Sigma_1 & \text{for } \vec{k}\in \text{Region I}(S) \\ \Sigma^{\rm imp}_P = \Sigma_0 - \Sigma_1 & \text{for } \vec{k}\in \text{Region II}(P). \end{cases} \tag{8}$$

The partial densities of states are

$$D_{S(P)}(\epsilon) = 2\times\int_{\vec{p}\in \rm I(II)} (dp)\,\delta(\epsilon-\epsilon_{\vec{p}}) \tag{9}$$

and the self-consistency equation from Eq. (2) is

$$G_0 = (G_S+G_P)/2,$$

$$G_1 = (G_S-G_P)/2, \tag{10}$$

with

$$G_{S(P)} = \int \frac{D_{S(P)}(\epsilon)d\epsilon}{\omega+\mu-\epsilon_{\vec{p}}-[\Sigma_0+(-)\Sigma_1]}. \tag{11}$$

D. Formalism for 4-site DCA in square lattice

After solving a 4-site impurity cluster problem, one gets (in the real-space basis)

$$\hat{G}^{\rm imp} = \begin{pmatrix} G_0 & G_1 & G_2 & G_1 \\ G_1 & G_0 & G_1 & G_2 \\ G_2 & G_1 & G_0 & G_1 \\ G_1 & G_2 & G_1 & G_0 \end{pmatrix} \quad \hat{\Sigma}^{\rm imp} = \begin{pmatrix} \Sigma_0 & \Sigma_1 & \Sigma_2 & \Sigma_1 \\ \Sigma_1 & \Sigma_0 & \Sigma_1 & \Sigma_2 \\ \Sigma_2 & \Sigma_1 & \Sigma_0 & \Sigma_1 \\ \Sigma_1 & \Sigma_2 & \Sigma_1 & \Sigma_0 \end{pmatrix}. \tag{12}$$

The partitioning of Brillouin zone in this case is given in Fig. 1(b). The four $\vec{K}$ points are (0,0), $(\pi,0)$, $(0,\pi)$, (π,π) which are labeled as S, P, D. Corresponding to these $\vec{K}$ points one gets four $\vec{R}$ as (0,0), (1,0), (0,1), and (1,1). The lattice self-energy is related to $\hat{\Sigma}^{\rm imp}$ by

$$\Sigma_S = \Sigma_0 + 2\Sigma_1 + \Sigma_2,$$

$$\Sigma_P = \Sigma_0 - \Sigma_2,$$

$$\Sigma_D = \Sigma_0 - 2\Sigma_1 + \Sigma_2. \tag{13}$$

The partial densities of states are

$$D^{(4)}_{S(P,D)}(\epsilon) = 4\int_{\vec{p}\in S(P,D)} (dp)\,\delta(\epsilon-\epsilon_{\vec{p}}), \tag{14}$$

where the superscript (4) is used to distinguish from the partial DOS in 2-site DCA. The self-consistency equations are

$$G_0 = (G_S+2G_P+G_D)/4,$$

$$G_1 = (G_S-G_D)/4,$$

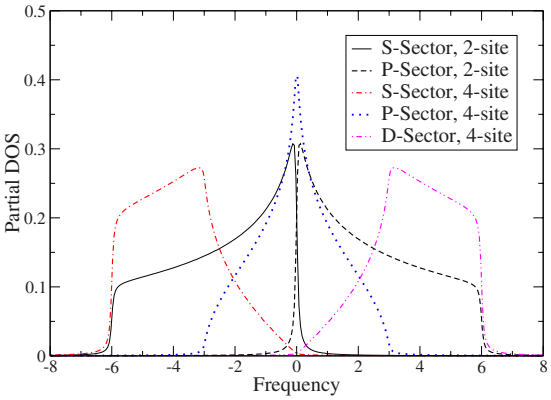

FIG. 2. (Color online) The PDOS for 2-site and 4-site DCA partitionings on the square lattice with nearest-neighbor hopping. The total bandwidth is 12.

$$G_2 = (G_S - 2G_P + G_D)/4, \tag{15}$$

with

$$G_{S(P,D)} = \int \frac{D_{S(P,D)}(\epsilon)d\epsilon}{i\omega_n + \mu - \epsilon - \Sigma_{S(P,D)}}. \tag{16}$$

E. Band structure and partial density of states

Throughout this paper we will consider the square and cubic lattices with only nearest-neighbor hopping and with hopping parameter adjusted so that the total bandwidth chosen is 12. For the square lattice with one S-like orbital per site, the band dispersion is

$$\epsilon_{\vec{k}} = -2t[\cos(k_x) + \cos(k_y)]. \tag{17}$$

The corresponding PDOS for 2-site and 4-site DCAs with bandwidth 12 (t=1.5 in this case) are shown in Fig. 2. For the cubic lattice with one S-like orbital per site, the band dispersion is

$$\epsilon_{\vec{k}} = -2t[\cos(k_x) + \cos(k_y) + \cos(k_z)]. \tag{18}$$

The manganite materials[13] are characterized by a pseudocubic lattice but because the important orbitals are transition-metal e_g orbitals, the hopping is direction dependent. The band dispersion is described by a matrix as

$$\hat{\epsilon}_{\vec{k}} = \epsilon_0\hat{e} + \epsilon_z\hat{\tau}_z + \epsilon_x\hat{\tau}_x, \tag{19}$$

where $\hat{e}$, $\hat{\tau}_x$, and $\hat{\tau}_z$ are unit and Pauli matrices;

$$\epsilon_0 = -t[\cos(k_x) + \cos(k_y) + \cos(k_z)],$$

$$\epsilon_z = -t\{\cos(k_z) - [\cos(k_x) + \cos(k_y)]/2\},$$

and

$$\epsilon_x = -t\frac{\sqrt{3}}{2}[\cos(k_x) - \cos(k_y)].$$

The PDOS for 2-site cubic lattice are plotted in Fig. 3.

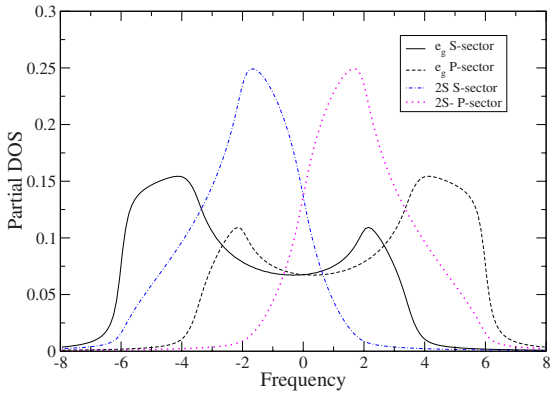

FIG. 3. (Color online) Partial DOS for $3D$, $2S$, and e_g bands.

III. POLARON PROBLEM AND ITS IMPURITY CLUSTER

A. Overview

In this section we briefly review the breathing mode polaron model and its solution by dynamical mean field theory. Based on the properties of this model, we provide two characterizations of the importance of short-ranged correlation.

The breathing mode coupling. The Hamiltonian for the polaron model is

$$H = \sum_{\langle ij\rangle,\alpha\beta} t_{ij}c_{i\alpha}^{\dagger}c_{j\beta} + \sum_i \left[Q_i n_i + \frac{Q_i^2}{2U}\right], \tag{20}$$

where α and β can be spin or orbital indices, Q_i is the local breathing mode distortion with U the restoring energy, and $n_i = \Sigma_\alpha c_{i\alpha}^{\dagger}c_{i\alpha}$ is the local charge density. Note that the oscillator coordinate Q is a purely classical variable. This model has been solved using S-DMFT in Ref 14. The main physical effect of the breathing mode Q_i is to trap electrons. In particular when the coupling U exceeds a density-dependent critical $U_c(n)$ the system becomes insulating at zero temperature. The physical interpretation of the insulating behavior is as follows: because a site with a higher density induces a lattice distortion which binds the electron and lowers the energy, the system eventually is phase separated into empty and maximally occupied sites where at empty sites there is no lattice distortion, while at maximally occupied site the local distortion is at its strongest value. The insulating behavior is a consequence of the classical phonon approximation. Quantum fluctuations of phonons would lead to a small but nonzero conductivity at nonrational N.

B. Solution by dynamical mean field theory

Local partition function. In any cluster-DMFT calculation, the impurity cluster problem is defined by a partition function. For the polaron model on an N_s site cluster, the local distortion fields are described by N_s classical fields Q_i which couple to a local density which is quadratic in fermionic operators. Because the model is quadratic in fermion operators, the fermionic degrees of freedom can be integrated out and the resulting partition function expressed as an integral over N_s classical fields

TABLE I. Gap opening critical coupling U_c for the polaron model on a square lattice with bandwidth 12 obtained from DCA with different cluster size.

Cluster size	1-site	2-site	4-site
U_c	~5	~3	3~3.5

$$Z^{\text{imp},N_s} = \int_{-\infty}^{\infty} \Pi_{i=1}^{N_s} dQ_i e^{-V(\{Q_i\})/T} \tag{21}$$

with

$$V(\{Q_i\}) = -2T\text{Tr}\log[\hat{a} - \text{diag}(Q_1, Q_2, \ldots, Q_{N_s})] + \frac{1}{2U}\sum_{i=1}^{N_s} Q_i^2. \tag{22}$$

Here, $\hat{a}$ is a $N_s \times N_s$ matrix composed of a set of Weiss functions $\{a_i\}$. The 2 in front of the trace accounts for two degenerate local orbitals.

For a 2-site cluster in the disordered phase, two sets of Weiss functions a_0, a_1 are needed and

$$\hat{a}^{\text{2-site}} = \begin{pmatrix} a_0 & a_1 \\ a_1 & a_0 \end{pmatrix}. \tag{23}$$

For a 4-site cluster, three sets of Weiss functions a_0, a_1, a_2 are required and

$$\hat{a}^{\text{4-site}} = \begin{pmatrix} a_0 & a_1 & a_2 & a_1 \\ a_1 & a_0 & a_1 & a_2 \\ a_2 & a_1 & a_0 & a_1 \\ a_1 & a_2 & a_1 & a_0 \end{pmatrix}. \tag{24}$$

The Weiss function, Green's function, and self-energies in real and imaginary axes are calculated using the procedure described in Ref. 14 and 15. The main quantity we will show is the spectral function $A(\omega)$. The zero in frequency ω is the Fermi energy. We define metal and insulator by the absence or presence of a gap at the Fermi level. To facilitate later comparisons, the total bandwidth is fixed at 12 for all band structure considered in this paper.

Defining the importance of short-ranged effects. There is no generally accepted measure of "the importance of short-ranged correlations." Here we provide a definition in the context of cluster dynamical mean field theory: because the single-site DMFT completely neglects the spatial correlation, we define the strength of the short-ranged effect in terms of the *deviation* of cluster results from single-site DMFT results. Two quantitative measurements are now stated. First, both single site and cluster DMFT require a critical (minimum) interaction strength, $U_c^{\text{1-site}}$ and U_c^{cluster}, to get an insulating phase at zero temperature, and the ratio $U_c^{\text{cluster}}/U_c^{\text{1-site}}$ (<1 generally) is a measure of the importance of short-ranged correlations. Second one can calculate the intersite phonon correlation function

$$\langle Q_i Q_j \rangle (\equiv \int_{-\infty}^{\infty} \Pi dQ_k [Q_i Q_j] e^{-V(\{Q_k\})/T}/Z^{\text{imp}}).$$

In single-site DMFT, $\langle Q_i Q_j \rangle = \langle Q_i \rangle \langle Q_j \rangle = 0$ while in cluster DMFT $\langle Q_i Q_j \rangle \neq 0$. Since that the number of intersite correlation functions increases exponentially when going to larger cluster size (including multisite correlations), we shall primarily use the reduction of U_c in this paper. However we note that these two measures are related—for the 2-site cluster calculation, smaller $U_c^{\text{cluster}}/U_c^{\text{1-site}}$ corresponds to larger $|\langle Q_1 Q_2 \rangle|$ (see Table III and IV).

C. Pole in self-energy

We shall see that in the models we solve the insulating phases are associated with polelike structures in the self-energy

$$\Sigma \sim \frac{V^2}{\omega - \Delta - i\gamma}, \tag{25}$$

characterized by pole amplitude V^2, pole position Δ, and damping γ which is small or zero. The presence of a pole is related to insulating behavior because insulating behavior is characterized by a gap, i.e., a region around the Fermi level (which we take to be 0) around which $\text{Im}[G(\vec{k}, \omega)] = 0$. If $\text{Im}[G] = 0$ then $\text{Im}[\Sigma] = 0$ except at poles.

A gap in the spectral function at ω implies both that $\text{Im}[\Sigma(\omega)] = 0$ and that there is no solution to $\text{Re}[G^{-1}(\vec{k}, \omega)]$

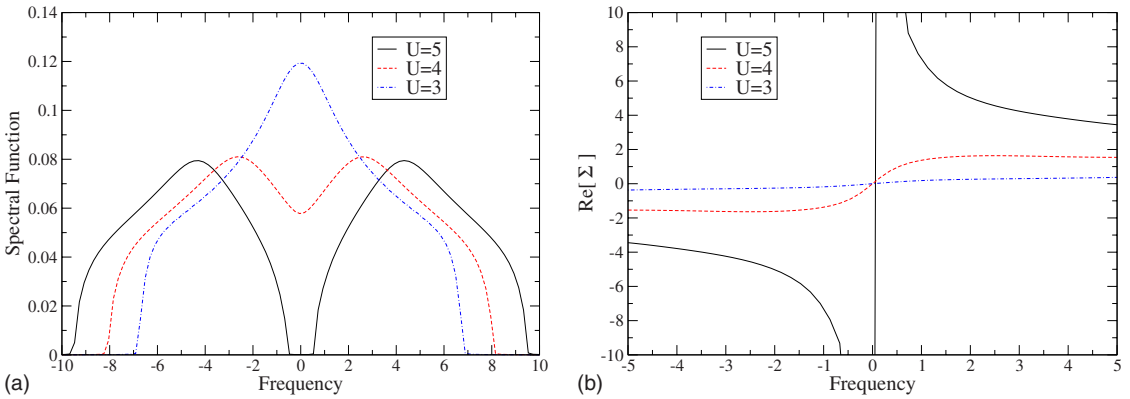

FIG. 4. (Color online) Results from single-site DMFT calculation for two-dimensional square lattice with nearest-neighbor hopping $t = 1.5$ (bandwidth 12), polaronic coupling [Eq. (20)], $U = 3, 4, 5$, and $T = 0.1$: (a) spectral functions; (b) real part of self-energies.

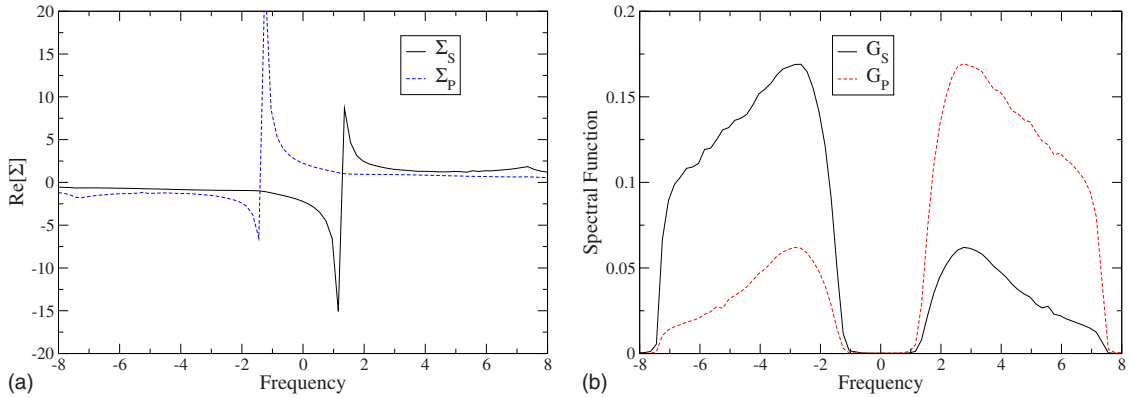

FIG. 5. (Color online) Results from 2-site DCA calculation for two-dimensional square lattice with nearest-neighbor hopping $t=1.5$ (bandwidth 12), polaronic coupling [Eq. (20)], $U=4$, and $T=0.1$. (a) Real part of self-energies for S and P sectors. (b) Partial spectral functions for S and P sectors.

$=0$. In the DCA approximation this equation may be written as

$$\omega - \epsilon_{\vec{k}} - \mathrm{Re}[\Sigma_{\vec{K}_i}(\omega)] = 0 \tag{26}$$

for each momentum sector $\vec{K}_i$ and for $\epsilon_{\vec{k}}$ in the allowed range corresponding to sector $\vec{K}_i$. If the main contribution of the self-energy is the pole, then the boundaries of the gap region can be obtained from the roots of $\omega-\epsilon-V^2/(\omega-\Delta)=0$, which are

$$\omega_{+(-)} = \frac{1}{2}[(\epsilon+\Delta)+(-)\sqrt{(\epsilon-\Delta)^2+4V^2}]. \tag{27}$$

Clearly a pole in Σ near the Fermi level implies a large magnitude of $\mathrm{Re}[\Sigma]$ at low ω, preventing any solution to Eq. (26) for the allowed range of $\epsilon_{\vec{k}}$. There are two interesting cases. If we consider density wave order at wave vector $\vec{Q}$ and neglect the long-ranged order by focusing on the diagonal elements of G, we find

$$\Sigma_{\mathrm{DW}}(\vec{p},\omega) \sim \frac{V^2}{\omega - \epsilon_{\vec{p}+\vec{Q}}} \tag{28}$$

(A broadened version of Σ_{DW} is the basis of the Lee-Rice-Anderson theory[16] of the pseudogap in thermally disordered charge-density waves).

Σ_{DW} expresses the physics of level repulsion: if $\epsilon_{\vec{p}+\vec{Q}} > \epsilon_{\vec{p}}$ then the presence of Σ_{DW} pushes the solution of Eq. (26) (which would be $\omega=\epsilon_{\vec{p}}$) to an energy lower than $\epsilon_{\vec{p}}$, while also creating a second lower weight solution at $\omega > \epsilon_{\vec{p}+\vec{Q}}$. We shall see that in many cases the cluster-DMFT theories, which replace self-energies by some sort of momentum averaged self-energies, lead to just this physics, with the self-energy corresponding to a $\vec{K}$ sector with $\epsilon_{\vec{k}}$ dominantly less than 0 having a pole at an energy $\Delta>0$, so that the effect of Σ is to push the states in this $\vec{K}$ sector away from $\omega\sim 0$. We interpret the self-energy as arising from a near resonant coupling to states in a complementary $\vec{K}$ sector [e.g., $\vec{K}+(\pi,\pi,\pi)$ sector]. We interpret this as the density wave (Slater-like) mechanism.

On the other hand, one sometimes finds cases where the self-energy corresponding to a given $\vec{K}$ sector has a pole at

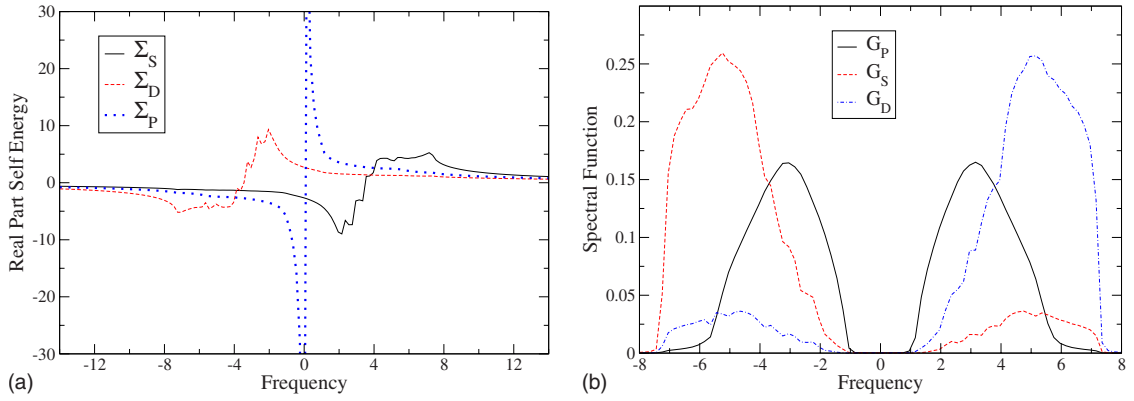

FIG. 6. (Color online) Results from 4-site DCA calculation for two-dimensional square lattice with nearest-neighbor hopping $t=1.5$ (bandwidth 12), polaronic coupling [Eq. (20)], $U=4$, and $T=0.1$. (a) Real part of self energies for S P and D sectors. (b) Partial spectral functions for S P and D sectors.

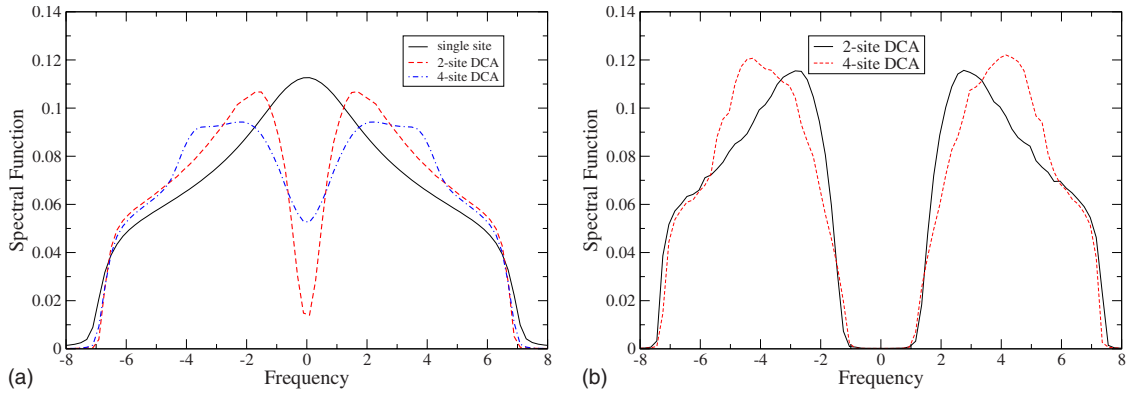

FIG. 7. (Color online) Spectral functions calculated by 2-site and 4-site DCA approximations for the two-dimensional square lattice with nearest-neighbor hopping $t=1.5$, polaronic coupling [Eq. (20)], (a) $U=3$ and $T=0.2$, and (b) $U=4$ and $T=0.1$.

an energy Δ in the middle of the allowed energy range arising from coupling to all $\vec{K}$ sectors. In that sector, the pole in self-energy pushes states away in both directions. We identify this as the Mott mechanism. There is clearly a continuum of behaviors connecting the Slater and Mott limits, but we will see that the physics can be reasonably clearly assigned.

Extracting pole parameters. The pole parameters—the position, the amplitude, and the damping—from $\Sigma \sim V^2/(\omega-\Delta+i\gamma)$ are obtained as follows. The position Δ is estimated by $\mathrm{Re}[\Sigma]=0$ (any Hartree contribution is absorbed into the chemical potential, which we define to be 0); the amplitude V^2 and damping δ are determined by fitting the $\mathrm{Re}[\Sigma]$ to $V^2(\omega-\Delta)/[(\omega-\Delta)^2+\gamma^2]$.

IV. HALF-FILLED CASE

A. Overview

In this section the DCA method with cluster size 1, 2, 4 is used to analyze the two-dimensional square lattice with nearest-neighbor hopping $t=1.5$ (bandwidth 12). The model displays a metal-insulator transition as the interaction U is increased beyond a critical value U_c, which as shown in Table I is in the range of $3\sim5$ depending on the cluster size.

The excitation spectra are obtained for different cluster sizes. The physics of the metal-insulator transition and the variations in results with cluster size are related to the behavior of poles in the self-energy. In the rest of this section we present and analyze the results for 1-, 2-, and 4-site DCA calculations for the local interaction range $U \lesssim U_c^{\text{1-site}}$ ($U_c^{\text{1-site}}$ is the gap opening U for single-site DMFT calculation).

TABLE II. the pole position, gap edge, and intersite phonon correlation for different polaronic coupling U obtained from 2-site DCA calculation on the two-dimensional square lattice with bandwidth 12.

U	3	4	5	10	15
S-pole location	1.21	1.31	1.51	2	2
Gap edge	~ 0	1	1.74	6.75	11
$-\langle Q_1 Q_2\rangle/U^2$	0.40	0.61	0.73	0.92	0.924

B. Single-site results

We first present the single-site DMFT calculation. Figure 4(a) shows the spectral functions for $U=3,4,5$ at $T=0.1$. The gap-opening interaction for the single-site calculation, $U_c^{\text{1-site}}$, is slightly less than 5. As discussed in the previous section, the insulating behavior is related to a pole in the self energy. This is shown in Fig. 4(b) which reveals at $U=3$ the real part of the self energy is very weak; at $U=4$ a strongly broadened pole begins to appear, and at $U=5$ an undamped pole occurs.

The self-energy sum rule for this model is $\int \frac{d\omega}{\pi}\mathrm{Im}[\Sigma(\omega)] = U^2$. By fitting Σ (not shown here) at $U=5$ we find the pole strength $V^2=7.5$ so that the pole contains roughly 30% of the total self-energy sum rule. As U is increased the fraction of the self-energy sum rule contained in the pole increases to 90% of the total at $U=10$ and 99% at $U=20$. However even for $U=5$ where there is a substantial nonpole contribution to $\mathrm{Im}[\Sigma]$, the size of the gap is to a good approximation given by inserting $\Sigma=V^2/\omega\sim 7.5/\omega$ into the quasiparticle equation Eq. (26).

C. 2-site results

In this subsection we show results from 2-site DCA calculation. We focus on $U=4$ where the solution is insulating but in the 1-site approximation would be metallic. Figure 5(a) shows the real part of the self-energy for S and P sectors at $U=4$ $T=0.1$ in for 2-site DCA method. The most prominent feature is poles. Comparison to Fig. 2 shows that the pole in the S sector (here $\Delta\sim 1.5$) lies above the energy range where the S sector PDOS is nonvanishing, while the pole in the P sector lies below the support of the P sector PDOS. As discussed previously, the pole pushes the main part of the S sector PDOS down in energy while generating some excitation at energies above the pole energy. The opposite effect occurs in the P sector. Therefore in the 2-site DCA the origin of the gap-opening transition is a coarse-grained (in momentum space) version of the Slater physics.

D. 4-site results

As in Sec. IV C we focus on the insulating solution. In the 4-site DCA calculation, there are three different sectors S, P,

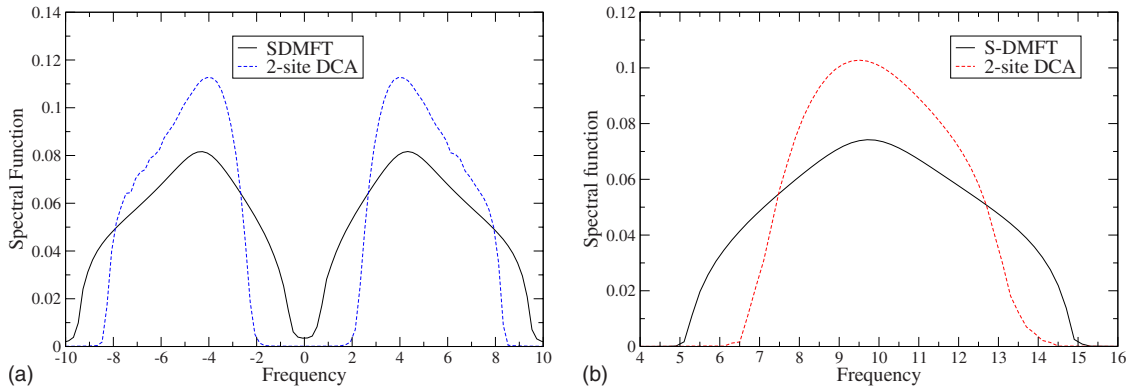

FIG. 8. (Color online) Spectral functions from S-DMFT and 2-site DCA calculation for the two-dimensional square lattice with nearest-neighbor hopping $t=1.5$, polaronic coupling (a) $U=5$, and (b) $U=10$, $T=0.1$, and $N=1$. For $U=10$ only the upper Hubbard band is shown.

and D in momentum space. Their self-energies and partial spectral functions are shown in Fig. 6. As seen from Fig. 2, the PDOS of S and D sectors barely touch each other and the poles obtained from 4-site DCA have exactly the same effect as the S and P sectors in the 2-site calculation—S and D sectors repel each other. However in the P sector the pole energy is zero and the physics is "Mott-like." We emphasize that in DCA equation all three sectors are coupled so states in the P sector are not isolated from states of other two sectors. Thus while the P sector bandwidth is a factor of two smaller than the total bandwidth, the 4-site $U_c^{\text{4-DCA}} \sim 3.5$ is about 70% of the single-site value.

We observe that the polaron model [local coupling $Q\hat{n} + \frac{1}{2}Q^2/U$, Eq. (20)] is in this respect different form the Hubbard model, where $U_c^{\text{4-site}} \sim 0.4 U_c^{\text{1-site}}$.[6,7] We further observe that the U-driven transition in the 4-site DCA approximation to the polaron model is continuous while in the Hubbard model the transition is strongly first order. In the Hubbard model the transition was associated with the dominance of a particular plaquette singlet state[6] not important here, suggesting that the smaller $U_c^{\text{4-site}}$ in the Hubbard model case is a manifestation of the strong short-ranged ordering effect.

E. Comparison between 2-and 4-site spectral functions

Now we compare spectral functions for 2-site and 4-site DCA calculations in Fig. 7. At $U=2$ (not shown) the spectral functions are similar. At $U=3$ ($\sim U_c^{\text{2-site}}$ but $< U_c^{\text{4-site}}$) the spectra are different; but by $U=4$ the spectra have again become very similar. As U continues to increase the difference between 2 and 4-site calculations remain small, but both remain different from the results of the single-site calculation: in the multisite case the gaps are larger and the gap edge more sharply defined. This is a consequence of short-ranged order (see also Table II, third row) and is demonstrated in Fig. 8 in which the results obtained from single-site DMFT and 2-site DCA are shown for $U=5$ and $U=10$. One sees that the sharp band edge remains at large U. Our finding is consistent with previous studies on nearly half-filled Hubbard model in the sense that 2-site and 4-site cluster calculations yield similar results for a wide range of U.[17,18]

V. T AND U DEPENDENCE

In this section we discuss the temperature and interaction dependence of the poles in the self-energies. As previously discussed, in both single-site and cluster-DMFT calculations, the insulating behavior can be traced back to a polelike structure in self-energy. The pole is characterized by its location Δ, amplitude V^2, and damping δ which we now analyze for different interaction strengths U and temperature T.

Figure 9 shows the temperature dependence of the density of states and the real part of the S sector self-energies calculated in the 2-site DCA approximation for $U=4$ (bandwidth 12). As the temperature is raised, the gap begins to fill in, and this change is accompanied by an obvious decrease in the size and sharpness of the pole structure. While the pole is not well separated from the other contributions to Σ, a simple fit yields a gradual decrease in the amplitude V^2 [Eq. (25)] from 13 at $T=0.1$ to 9 at $T=0.3$, and a rapid increase in the damping γ from negligible at $T=0.1$ to $\gamma=0.3$ at $T=0.2$ to $\gamma=0.6$ at $T=0.3$. The shift in pole position is very small. Thus the main contribution to the destruction of the insulating phase is a broadening of the pole. A similar conclusion is found in the 4-site calculation (not shown here). The T independence of the pole position is in contrast to the results of Ref. 11 who found the pole position was temperature dependent, tracking the cluster spin correlation function. We believe this is a difference between the strong-coupling limit considered in Ref. 11 and the intermediate coupling studied here.

We next discuss the U dependence in DCA calculation. We begin with the strong-coupling limit in which the excitations are expected to be roughly $+(-)U$. From Eq. (27), when amplitude of the pole is very large compared to both the pole location Δ and the half-bandwidth of noninteracting spectrum Λ, the excitations are roughly $\omega_{+(-)} \sim +(-)V$. Therefore in this limit one expects the pole amplitude is U^2 and the location of the pole is well within the gap, i.e., $|\Delta| \ll U$ (see the first row of Table II). As U is decreased, the band gap and the pole energies both decrease, but the band gap decreases much faster so that for the intermediate U the pole in the self-energy actually lies within the continuum of excited states (see the first and second rows of Table II) so it is technically not a pole but is a resonance. Thus a pole in the

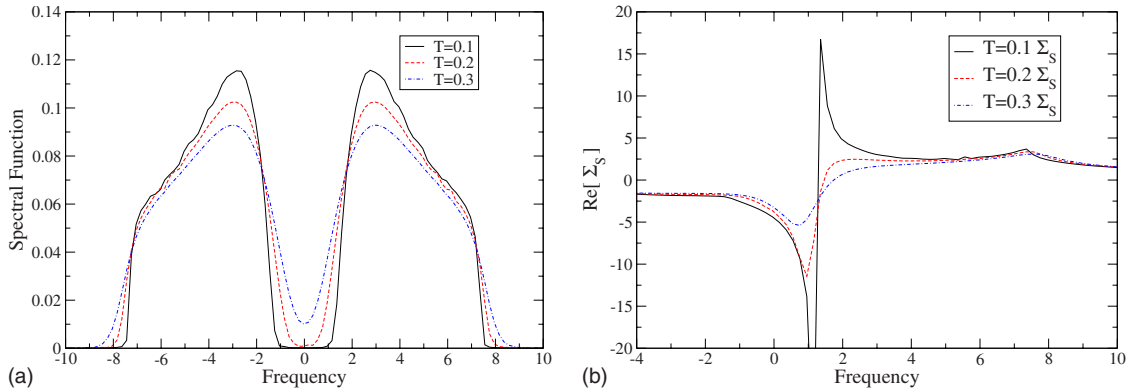

FIG. 9. (Color online) Spectral functions (left panel) and real part of self-energy (right panel) from 2-site DCA calculation for the two-dimensional square lattice with nearest-neighbor hopping $t=1.5$ (bandwidth 12), polaronic coupling $U=4$, and $T=0.1-0.3$.

self-energy is not necessary for insulating behavior. We also find that the "pole" energy does not have a simple relation to the intersite phonon correlation $\langle Q_1 Q_2 \rangle$ (third row of Table II). This is again in contrast to results of Ref. 11, which found via an approximate analytical calculation that in the Hubbard model the pole energy was proportional to the spin correlation function $\langle S_1 \cdot S_2 \rangle$. We believe the difference arises from the coupling strength. The U dependence is summarized in Table II whose first row gives the S sector pole position obtained from 2-site DCA calculation for different U at $T=0.1$, second row the gap edge, and third row the intersite correlation function.

VI. FILLING AND CLUSTER SIZE

A. Overview

In this section we discuss band filling effects in cluster-DMFT theory. The basic finding is that the filling determines the minimum cluster size required to provide a significant difference between single-site and cluster-DMFT results—the minimum size increases as the system is doped from the half filling. In this section we restrict ourselves to the square lattice only.

B. General filling 2-site

In this subsection we compare the doping dependence found in single-site and 2-site DCA for $U=5$ above the critical value for insulating behavior in both approximations. The discussion of Fig. 8 in Sec IV showed the pronounced differences between single-site and cluster-DMFT calculations at density $N=1$. For the very low doping $N=0.2$ on the other hand, the single-site DMFT and 2-site DCA behave very similarly. Figure 10(a) shows that within DCA poles in self-energies in the two sectors are almost identical, and are quite close to that in single-site DMFT. Consequently the spectral functions obtained from both methods are very similar [Fig. 10(b)]. This can be understood as follows. At $N=0.2$, the Fermi energy only lies deep inside the S-sector PDOS, the P sector is irrelevant, and the DCA calculation within the S sector is just like a single-site DMFT calculation.

C. Near quarter filling, 2-site, and 4-site

In the classical polaronic model, insulating behavior can occur at any density if the interaction is strong enough. In this section we show that the Slater mechanism of shifting of states in k space can lead to insulating behavior at smaller U if the band filling is such that one of the sectors is mostly filled, while the adjacent one with higher energies is nearly empty. However these cluster size effects diminish rapidly in importance as the density is moved away from commensurate values. The left panel of Fig. 11 compares the results from 1-site, 2-site, and 4-site DCA approximations to the two-dimensional square lattice with nearest-neighbor hop-

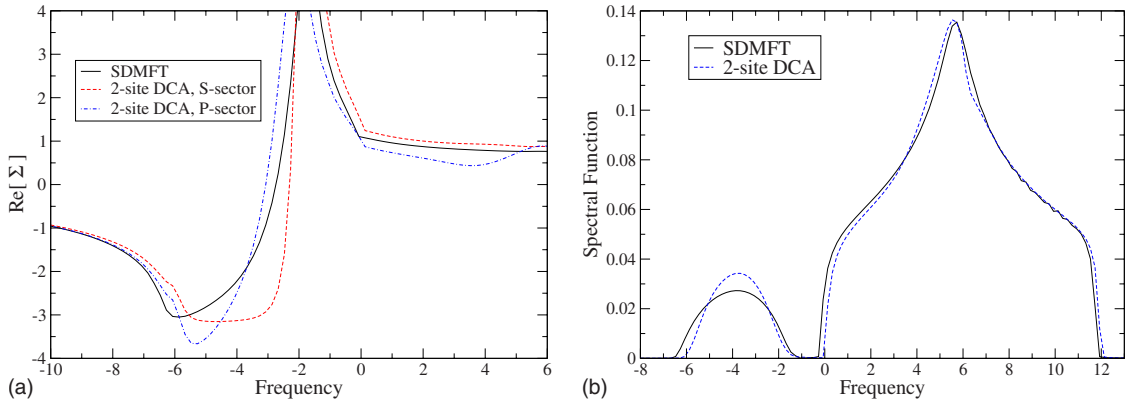

FIG. 10. (Color online) Self-energy (left panel) and spectral function (right panel) calculated from single-site (solid line) and 2-site DCA (dashed line) approximations for the square lattice with nearest-neighbor hopping $t=1.5$, polaronic coupling $U=5$, $T=0.1$ at $N=0.2$.

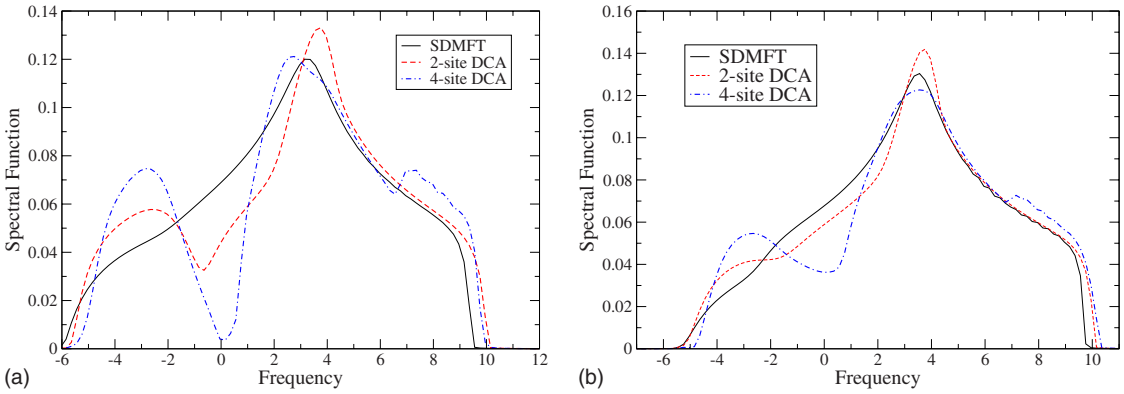

FIG. 11. (Color online) Spectral functions calculated by single-site DMFT, 2-site, and 4-site DCA approximations at $U=4$, $T=0.1$, (a) $N=0.5$ and (b) $N=0.4$.

ping at density $N=0.5$ and intermediate U. The four-site approximation produces a clearly insulating behavior, the two site gives a moderate "pseudogap," and the single-site approximation yields results very similar to the noninteracting model. The right panel of Fig. 11 shows that the differences decreases rapidly as the doping is moved from this commensurate value.

To unravel the origin of the insulating behavior we consider the self-energies for the 4-site DCA shown in Fig. 12. The right panel shows a clear pole in the S sector, lying at an energy slightly above the chemical potential μ and substantially above the average energy of S sector $\sim\mu-0.93$. This pole gives rise to the Slater effect of pushing most of S sector states down in energy. Consequently the P and D sector self-energies lie below the P and D PDOS and push these states up, leaving the gap observed in Fig. 11.

By contrast the left panel of Fig. 12 shows for the 2-site DCA an interesting hybrid behavior. The P sector pole lies below the P-sector PDOS and pushes these states up. The S sector pole lies roughly at $\mu-1$, below the average energy of S PDOS $\langle\epsilon\rangle_S^{2\text{-site}}=\mu+0.95$ and acts in a Mott-like fashion, splitting the band into two.

VII. ROLE OF PARTIAL DENSITY OF STATE

A. Overview

In this section we establish a relation between the PDOS defined in Eq. (3) and the differences between cluster and single-site DMFT calculations. In essence, the more overlap between PDOS, the more similar are the single-site and cluster calculations. To measure the overlap between PDOS of two sectors, we first compute the overlap $O_{ij}\equiv\int d\epsilon D_i(\epsilon)D_j(\epsilon)$. One can also use the first two moments of the partial DOS. For PDOS i, $\langle\epsilon\rangle_i=\int d\epsilon\epsilon D_i(\epsilon)$ gives the average position of the partial DOS while $\sigma_i=\sqrt{\langle\epsilon^2\rangle_i-\langle\epsilon\rangle_i^2}$ tells how spread the PDOS is. The overlap is related to $\langle\epsilon\rangle_i/\sigma_i$. We consider two examples. First we compare 2-site DCA and 2-site cellular-DMFT solutions to the polaron model on the square lattice. Second, we compare the approximations to two models involving the polaron model defined on a cubic lattice: one has two degenerate S-like orbitals per site the other two e_g orbitals, with dispersions given in Eq. (18) and Eq. (19), respectively. We mention that different DCA tilings lead to different PDOS which are the only lattice information required in the DCA equations; therefore our conclusions here serve as the same mathematical origins for differences between different DCA tiling schemes which we do not present in this paper.

B. Difference between 2-site DCA and 2-site CDMFTs for 2D square lattice

In this subsection we compare the two site DCA and cellular-DMFT solutions to the polaron model defined on the square lattice. As discussed in Sec II and Appendix A the

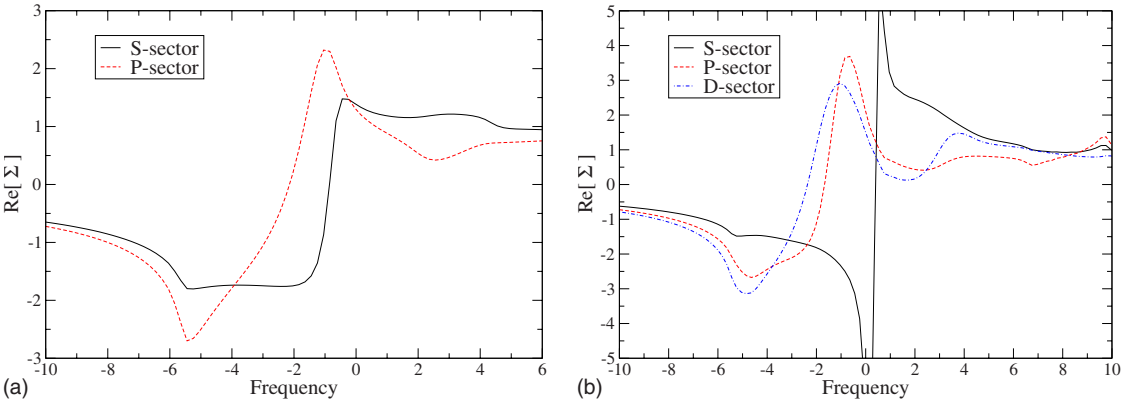

FIG. 12. (Color online) Self-energies calculated by (a) 2-site and (b) 4-site DCA approximations for the two-dimensional square lattice with bandwidth 12 at $U=4$, $T=0.1$, $N=0.5$.

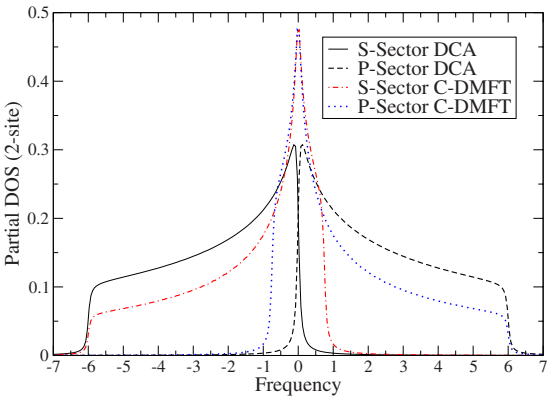

FIG. 13. (Color online) Partial DOS for 2-site DCA and Cellular-DMFT on the square lattice with nearest-neighbor hopping $t=1.5$ (bandwidth 12). U_c for 1-site DMFT, 2-site cellular DMFT, and 2-site DCA approximations are roughly 5, 4, and 3, respectively.

mean field equations may be expressed in the same form as

$$G_{S,P}^{\text{imp}} = \int d\epsilon \frac{D_{S,P}(\epsilon)}{\omega - \epsilon - \Sigma_{S,P}(\omega)}. \tag{29}$$

The two approximations are distinguished by the differences in PDOS, shown in Fig. 13. In the DCA case two PDOS do not overlap (the small apparent overlap is the result of numerical broadening); in the cellular DMFT the overlap is seen to be more substantial. Quantitative information on the overlaps is given in Table III

To further explore the difference we show in Fig. 14 the spectral functions calculated at $U=4$ and at the relatively high $T=0.2$. The DCA calculation reveals a well-defined gap, whereas the cellular DMFT reveals a weak pseudogap which will evolve to a small true gap as $T\to 0$. As seen from Eq. (29) these differences can arise mathematically only from the difference in PDOS.

Solving the equations reveals that the gap opening U of single-site DMFT at half filling is $U_c^{\text{1-site}} \sim 5$ (total bandwidth is 12), for 2-site cellular DMFT $U^{\text{2-Cellular}} \sim 4$, and for 2-site DCA, $U_c^{\text{2-DCA}} \sim 3$. The difference shows that the DCA expresses short-ranged correlations more strongly than the cellular DMFT.

C. 3D e_g and 2S band

In this section we compare the results of applying the DCA approximation to two orbitally degenerate models defined on a cubic lattice: the S-orbital model, with two degenerate bands of dispersion given in Eq. (18) and the e_g model, appropriate to the colossal magnetoresistance manganites, with dispersion given by the eigenvalues of Eq. (19). We choose the bandwidth to be 12 for both bands. The corresponding PDOS are shown in Fig. 3 and the overlaps are given in Table IV.

TABLE III. The overlap information of PDOS of S and P sectors for DCA and cellular DMFT on the square lattice with bandwidth 12. $\langle\epsilon\rangle_{S(P)}$ and $\sigma_S=\sigma_P$ are the average energy and the standard deviation of $S(P)$ PDOS. $U_c^{n\text{-site}}$ is the gap opening U for n-site cluster calculation. $\langle Q_1 Q_2\rangle$ is the intersite phonon correlation function defined in Sec. III B.

	O_{SP}	$\langle\epsilon\rangle_S=-\langle\epsilon\rangle_P$	$\sigma_S=\sigma_P$	$\frac{U_c^{\text{2-site}}}{U_c^{\text{1-site}}}$	$-\frac{\langle Q_1 Q_2\rangle}{U^2}\big\vert_{T=0.2,\ U=3}$
DCA	0	−2.41	1.82	~0.6	0.42
Cellular-DMFT	0.15	−1.48	1.89	~0.8	0.19

We see that the e_g band has larger PDOS overlap than the S band and thus one expects a smaller short-ranged correlation for the e_g case. Indeed, for 2S band $(U_c^{\text{1-site}} \sim 4) U_c^{\text{2-DCA}}/U_c^{\text{1-site}} \sim 3/4 = 0.75$ while for $e_g (U_c^{\text{1-site}} \lesssim 6) U_c^{\text{2-DCA}}/U_c^{\text{1-site}} \sim 5/6 = 0.83$. The corresponding spectral functions are provided in Fig. 15. We observed that in the insulating region the DCA leads to a larger gap and sharper band edge than the single-site DMFT, but the differences are less in the e_g case.

VIII. SUMMARY AND DISCUSSION

We first summarize our findings. The cluster-DMFT calculation reduces the critical interaction strength to open a gap. The magnitude of this is introduced as a quantitative measure of the importance of short-ranged correlation. The partial density of states (PDOS) and the filling of the system are two crucial quantities in the cluster-DMFT calculations. The reduction in critical U in cluster calculations is mainly caused by the momentum-dependent pole structure in self energies which pushes PDOS around Fermi energy away from each other. Similarly we find that significant differences between single-site and cluster calculations only occur when the Fermi energy involves several PDOS (2 at least). For example in the square lattice, the 2-site produces small U insulating behavior for half-filling problem but differs little from single-site DMFT for quarter filling. Obtaining a small U insulating state in the quarter filling requires a 4-site cluster. We show that when the cluster size is large enough, a

TABLE IV. The overlap information of PDOS of S and P sectors for S [Eq. (18)] and e_g [Eq. (19)] bands on the cubic lattice with bandwidth 12. $\langle\epsilon\rangle_{S(P)}$ and $\sigma_S=\sigma_P$ are the average energy and the standard deviation of $S(P)$ PDOS. $U_c^{n\text{-site}}$ is the gap opening U for n-site cluster calculation. $\langle Q_1 Q_2\rangle$ is the intersite phonon correlation function defined in Sec. III B.

	O_{SP}	$\langle\epsilon\rangle_S(=-\langle\epsilon\rangle_P)$	$\sigma_S(=\sigma_P)$	$\frac{U_c^{\text{2-site}}}{U_c^{\text{1-site}}}$	$-\frac{\langle Q_1 Q_2\rangle}{U^2}\big\vert_{T=0.2,\ U=5}$
2S-like band	0.044	−1.84	1.8	~0.75	0.74
e_g band	0.052	−1.82	2.98	~0.83	0.42

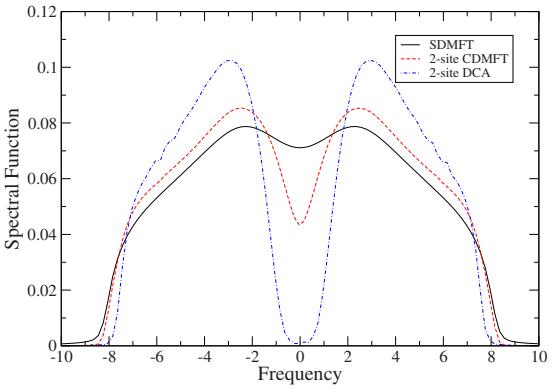

FIG. 14. (Color online) 2-site cellular-DMFT and DCA spectral functions calculated for the square lattice with nearest-neighbor hopping $t=1.5$ at half-filling polaronic coupling $U=4$, $T=0.2$. The DCA result is more insulating (having smaller density of state around the Fermi energy) than cellular-DMFT.

large separation between PDOS around Fermi energy implies a strong short-ranged effect. One notes that the difference between single-site and cluster-DMFT results becomes pronounced for the range of U where $\lesssim U_c^{\text{1-site}}$, above which the cluster calculations lead to a larger gap and sharper band edge. These features persist in the strong U limit and are consequences of the short-ranged correlation included in the cluster approximation.

The use of cluster-DMFT methods to study metal-insulator transitions at carrier concentrations different from half filling is an intriguing issue. Our results suggest that the cluster size must be tuned according to the filling to be studied. Roughly filling $1/N_s$ requires an N_s-site cluster. Thus for example study of the interesting phenomena associated with "half-doped" manganites (one carrier for every two twofold degenerate Mn orbitals, 1 electron per 4 orbitals, quarter filling), at least a 4-site cluster is required. The physics of the metal-insulator transitions at $N \neq 1$ is found generally to be Slater-like, arising from the separation in energy of k space sectors.

A generic result is that N_s-site ($N_s > 1$) cluster-DMFT calculations predict smaller critical U for the gap-opening (metal-insulator) transition than does the single-site approximation. Although various effects occur, we find that generically the most important role is played by a Slater-like effect. The calculation is most naturally viewed in terms of momentum-space sectors, and the dominant contribution to the insulator behavior is given by the pole structures in the self-energy which act to open gaps between the different momentum sectors.

ACKNOWLEDGMENTS

We thank Jie Lin, Xin Wang, and Hung The Dang for helpful discussion. This work is supported by DOE through Grant No. ER 46169.

APPENDIX A: PDOS OF CELLULAR-DMFT APPROXIMATION

In this appendix we derive the partial density of states for 2-site cellular-DMFT approximation for square lattice with nearest-neighbor hopping t. We begin by casting these two methods in the same formalism. Once the 2-site impurity cluster problem is solved, one gets Eq. (7). The self-consistency equation for both 2-site DCA and cellular-DMFT can be expressed in the same form similar to Eq. (1) as

$$\begin{pmatrix} G_0 & G_1 \\ G_1 & G_0 \end{pmatrix} = 2\int_{\vec{k}\in \mathrm{I}} (dk) \times \left[\omega + \mu - \begin{pmatrix} \Sigma_0 & \psi_{\vec{k}} + \Sigma_1 \\ \psi_{\vec{k}}^* + \Sigma_1 & \Sigma_0 \end{pmatrix} \right]^{-1}. \tag{A1}$$

Note that Region I is also the reduced Brillouin zone as depicted in Fig. 1(b). Choice of $\psi_{\vec{k}}$ distinguishes DCA and CDMFT. For DCA, $\psi_{\vec{k}} = \epsilon_{\vec{k}} = -2t(\cos k_x + \cos k_y)$; for CDMFT, $\psi_{\vec{k}} = \phi_{\vec{k}} \equiv -t[1 + e^{-2ik_x} + e^{-2i(k_x - k_y)} + e^{-2i(k_x + k_y)}]$ [see Eq. (10) in Ref. 11]. The partial density of states in this formalism is defined as

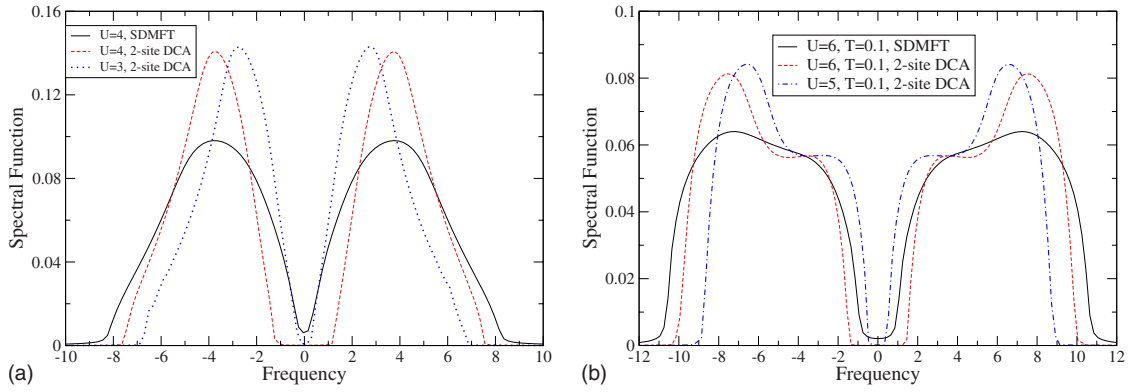

FIG. 15. (Color online) Spectral functions for the coupling close to the gap opening U_c. (a) For two degenerate S band with bandwidth 12, the $U_c^{\text{1-site}} \sim 4$ (solid) and $U_c^{\text{2-DCA}} \sim 3$ (dashed). (b) For e_g band with bandwidth 12, the $U_c^{\text{1-site}} \sim 6$ (solid) and $U_c^{\text{2-DCA}} \sim 5$ (dashed). Those curves are calculated at $T=0.1$.

$$D_{S(P)}(\epsilon) = \frac{2}{\pi} \times \int_{\vec{k}\in \mathrm{I}} (dk) \left[\epsilon - i0^+ - \begin{pmatrix} 0 & \psi_{\vec{k}} \\ \psi^*_{\vec{k}} & 0 \end{pmatrix} \right]^{-1}_{11(22)}. \tag{A2}$$

Note that the off-diagonal terms are zero for both cases. For $\psi_{\vec{k}} = \epsilon_{\vec{k}}$ one retains the definition in DCA; for $\psi_{\vec{k}} = \phi_{\vec{k}}$, one obtains the PDOS in cellular DMFT as

$$D(\epsilon)_{S(P)} = 2 \times \int_{\vec{k}\in \mathrm{I}} (dk)\, \delta(\epsilon - (+)\mathrm{Re}[\phi_{\vec{k}}]). \tag{A3}$$

APPENDIX B: STRONG-COUPLING ZERO-TEMPERATURE LIMIT IN 2-SITE DCA

In this appendix we analyze the polaron problem in the large-U zero-temperature limit. To facilitate the calculation, we assume that the partial density of states for S and P sectors to be semicircular with the average position at negative and positive α, i.e.,

$$D_{S(P)}(\epsilon) = \frac{1}{2\pi t^2} \sqrt{4t^2 - (\epsilon + (-)\alpha)^2} \tag{B1}$$

because of the analytical expressions. We will show that in this limit, the self-energies in S and P sectors indeed have pole as

$$\Sigma_{S(P)}(\omega) = \frac{U^2}{\omega - (+)\Delta} \tag{B2}$$

with the pole $\Delta = \alpha$.

We first solve the impurity cluster problem. Following the notation in Sec. III, in the $T=0$ large-U limit, (Q_1, Q_2) are either $(+U, -U)$ or $(-U, +U)$. Averaging these two configurations, one obtains

$$\hat{G}^{\mathrm{imp}} = \frac{1}{a_0^2 - a_1^2 - U^2} \begin{pmatrix} a_0 & -a_1 \\ -a_1 & a_0 \end{pmatrix} \tag{B3}$$

and interpreting

$$G^{\mathrm{imp}}_{S(P)} = \frac{1}{a_0 + (-)a_1 - U^2/[a_0 - (+)a_1]}. \tag{B4}$$

The self-energy is obtained by $\hat{\Sigma} = \hat{a} - (\hat{G}^{\mathrm{imp}})^{-1}$. After a little algebra, one gets

$$\Sigma_{S(P)} = \frac{U^2}{a_0 - (+)a_1}. \tag{B5}$$

Using these self-energies, the lattice Green's function for S sector is

$$\begin{aligned} G^{\mathrm{lat}}_S(\omega) &= \int \frac{D_S(\epsilon) d\epsilon}{\omega - \epsilon - \Sigma_S} \\ &= \frac{1}{2t^2}[(\omega + \alpha - \Sigma_S) - \sqrt{(\omega + \alpha - \Sigma_S)^2 - 4t^2}] \\ &\overset{\omega\to\infty}{\to} 1/(\omega + \alpha - \Sigma_S). \end{aligned} \tag{B6}$$

Similarly $G^{\mathrm{lat}}_P(\omega) \sim 1/(\omega - \alpha - \Sigma_P)$. Comparing the lattice and local Green's function, one gets $a_0 + (-)a_1 = \omega + (-)\alpha$; thus

$$\Sigma_{S(P)} = \frac{U^2}{a_0 - (+)a_1} \sim \frac{U^2}{\omega - (+)\alpha}. \tag{B7}$$

[1] M. Imada, A. Fujimori, and Y. Tokura, Rev. Mod. Phys. **70**, 1039 (1998).
[2] J. C. Slater, Phys. Rev. **82**, 538 (1951).
[3] N. F. Mott, Proc. Phys. Soc. London **49**, 36 (1937).
[4] A. Georges, G. Kotliar, W. Krauth, and M. Rezenberg, Rev. Mod. Phys. **68**, 13 (1996).
[5] T. Maier, M. Jarrell, T. Pruschke, and M. H. Hettler, Rev. Mod. Phys. **77**, 1027 (2005).
[6] E. Gull, P. Werner, X. Wang, M. Troyer, and A. J. Millis, EPL **84**, 37009 (2008).
[7] H. Park, K. Haule, and G. Kotliar, Phys. Rev. Lett. **101**, 186403 (2008).
[8] G. Kotliar, S. Y. Savrasov, G. Palsson, and G. Biroli, Phys. Rev. Lett. **87**, 186401 (2001).
[9] M. H. Hettler, A. N. Tahvildar-Zadeh, M. Jarrell, T. Pruschke, and H. R. Krishnamurthy, Phys. Rev. B **58**, R7475 (1998).
[10] T. D. Stanescu and G. Kotliar, Phys. Rev. B **74**, 125110 (2006).
[11] A. Fuhrmann, S. Okamoto, H. Monien, and A. J. Millis, Phys. Rev. B **75**, 205118 (2007).
[12] K. Haule and G. Kotliar, Phys. Rev. B **76**, 104509 (2007).
[13] in *Colossal magnetoresistive oxides*, edited by Y. Tokura (Gordon and Breach, New York, 2000).
[14] A. J. Millis, R. Mueller and B. I. Shraiman, Phys. Rev. B **54**, 5389 (1996).
[15] S. Okamoto, A. Fuhrmann, A. Comanac, and A. J. Millis, Phys. Rev. B **71**, 235113 (2005).
[16] P. A. Lee, T. M. Rice, and P. A. Anderson, Phys. Rev. Lett. **31**, 462 (1973).
[17] Y. Z. Zhang and M. Imada, Phys. Rev. B **76**, 045108 (2007).
[18] M. Ferrero, P. S. Cornaglia, L. De Leo, O. Parcollet, G. Kotliar, and A. Georges, arXiv:0806.4383 (unpublished).